JACS
JOURNAL OF THE AMERICAN CHEMICAL SOCIETY

Article

pubs.acs.org/JACS

A Dynamic Structural Model of Expanded RNA CAG Repeats: A Refined X-ray Structure and Computational Investigations Using Molecular Dynamics and Umbrella Sampling Simulations

Ilyas Yildirim,*[,†] HaJeung Park,[‡] Matthew D. Disney,*[,§] and George C. Schatz*[,†]

[†]Department of Chemistry and International Institute for Nanotechnology, Northwestern University, Evanston, Illinois 60208, United States

[‡]Translational Research Institute and [§]Department of Chemistry, The Scripps Research Institute, Jupiter, Florida 33458, United States

Supporting Information

ABSTRACT: One class of functionally important RNA is repeating transcripts that cause disease through various mechanisms. For example, expanded CAG repeats can cause Huntington's and other disease through translation of toxic proteins. Herein, a crystal structure of r[5′UUGGGC-(CAG)$_3$GUCC]$_2$, a model of CAG expanded transcripts, refined to 1.65 Å resolution is disclosed that shows both anti−anti and syn−anti orientations for 1 × 1 nucleotide AA internal loops. Molecular dynamics (MD) simulations using AMBER force field in explicit solvent were run for over 500 ns on the model systems r(5′GCGCAGCGC)$_2$ (MS1) and r(5′CCGCAGCGG)$_2$ (MS2). In these MD simulations, both anti−anti and syn−anti AA base pairs appear to be stable. While anti−anti AA base pairs were dynamic and sampled multiple anti−anti conformations, no syn−anti ↔ anti−anti transformations were observed. Umbrella sampling simulations were run on MS2, and a 2D free energy surface was created to extract transformation pathways. In addition, an explicit solvent MD simulation over 800 ns was run on r[5′GGGC(CAG)$_3$GUCC]$_2$, which closely represents the refined crystal structure. One of the terminal AA base pairs (syn−anti conformation), transformed to anti−anti conformation. The pathway followed in this transformation was the one predicted by umbrella sampling simulations. Further analysis showed a binding pocket near AA base pairs in syn−anti conformations. Computational results combined with the refined crystal structure show that global minimum conformation of 1 × 1 nucleotide AA internal loops in r(CAG) repeats is anti−anti but can adopt syn−anti depending on the environment. These results are important to understand RNA dynamic-function relationships and to develop small molecules that target RNA dynamic ensembles.

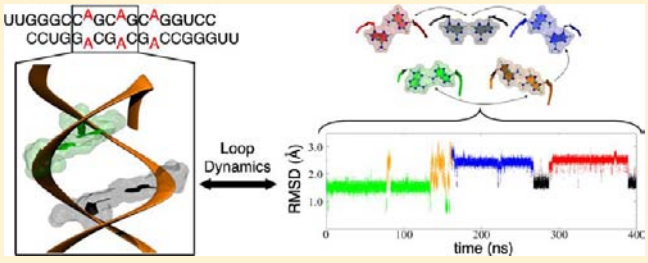

INTRODUCTION

Many diseases are caused by transcripts that contain expanded repeats. The physiological consequences of these expansions, and thus the mechanism of disease, are varied. For example, r(CUG) expansions [r(CUG)^{exp}] in the 3′-untranslated region (UTR) of the dystrophia myotonica protein kinase (*DMPK*) mRNA cause myotonic dystrophy type 1, while myotonic dystrophy type 2 is caused by an expansion of r(CCUG) [r(CCUG)^{exp}] in intron 1 of the zinc-finger 9 (*ZNF9*) protein mRNA. These diseases are characterized by muscle weakness and slow relaxation of muscles after contraction.[1,2] Fragile X-associated tremor ataxia syndrome (FXTAS) is caused by 50∼200 CGG repeats [r(CGG)^{exp}] in the 5′ UTR of the fragile X mental retardation 1 (*FMR1*) gene.[3−5] In each of these cases, the RNAs are in a noncoding region and are not translated into protein. Thus, disease is caused by an RNA gain-of-function.[1,6,7] In this mechanism, expanded repeats sequester proteins, typically ones involved in pre-mRNA splicing regulation, affecting their function. Muscleblind-like 1 protein (MBNL1) is sequestered and inactivated by r(CUG)^{exp} and r(CCUG)^{exp}, while Sam68 is inactivated by r(CGG)^{exp}.

In contrast to the above cases, expansions of CAG repeats [r(CAG)^{exp}] that cause disease are typically found in the coding regions of mRNAs. For example, r(CAG)^{exp} have been found in Huntingtin (*HTT*), androgen receptor (*AR*), spinocerebellar ataxia (*SCA*), and atrophin-1 (*ATN1*) genes and cause Huntington disease (HD), spinal and bulbar muscular atrophy (SBMA), spinocerebellar ataxia type 1 (SCA1), and dentatorubral-pallidoluysian atrophy (DRPLA), respectively. Since r(CAG)^{exp} is in the coding region of these transcripts, it is translated into toxic polyglutamine (polyQ) proteins that cause disease.[1,8−12]

More recently it has also been shown that r(CAG)^{exp} in coding regions can also sequester proteins such as MBNL1 and contribute to neurodegeneration.[13−15] Moreover, expanded

Received: November 11, 2012
Published: February 26, 2013

repeats in UTRs can be translated via a repeat-associated non-ATG translation.[16] Thus, although the disease mechanisms described above for each type of repeat are the most well established, it is not as clear-cut as it once appeared, and the interplay of RNA and protein toxicities may ultimately cause disease.

In order to gain insights into the role of RNA structure in these diseases, various approaches have been used to gain structural information. For example, chemical and enzymatic probing has shown that triplet repeat expansions form expanded hairpin structures with 1 × 1 nucleotide internal loops closed by GC pairs.[17] For several of these repeats, high-resolution structural information has been obtained through refinement of NMR spectral or X-ray crystallographic data.[18−23]

The structure of a model of r(CAG)^{exp} has been reported by Kiliszek et al.,[23] who studied the structure of the RNA duplex $(GGCAGCAGCC)_2$. They reported that the adenosines are in the anti conformations with a single C2−H2···N2 hydrogen bond, with significant distortions compared to a standard Watson−Crick paired duplex. This work did not identify fluxional behavior characteristic of large amplitude motions that might be expected for a 1 × 1 nucleotide internal loop. Information about such motions could improve our understanding of the conformations that toxic repeating transcripts adopt and how these conformations affect the binding of protein or small molecules.[24,25] Thus, the conformational flexibility of r(CAG) repeat-containing duplexes is of significant interest.[26]

Computational technology is an emerging scientific tool that can make useful predictions of the atomic details of structure as well as of RNA dynamics. Such studies are described herein and utilized to study the conformational heterogeneity of r(CAG) repeats. Methods such as residue-centered force fields (coarse-grained),[27] atom-centered force fields (AMBER,[28] CHARMM,[29,30] and GROMOS[31]), approximate quantum mechanics,[32,33] and mixed quantum-mechanics/molecular mechanics (QM/MM)[34−41] are typically used for predicting the structure and dynamics of RNA. Molecular mechanics force fields are computationally economical such that molecular dynamics (MD) simulations on the microsecond or faster time scales are possible.[42−46] Application of these methods allows for comparing the structural and thermodynamic properties of nucleic acids with experiments.[47−52] Free energy calculations are particularly important because free energies control a reaction coordinate. Combined with the weighted histogram analysis method (WHAM),[53,54] umbrella sampling[55−58] is a powerful computational approach to extract the free energy landscape along multiple reaction coordinates such as base opening[59] and base flipping[60−62] that can occur in DNA and RNA.

In this paper, we present the crystal structure of a self-complementary RNA duplex, r[5′UUGGGC(CAG)$_3$GUCC]$_2$ [a model of r(CAG)^{exp})], refined to 1.65 Å resolution [r(3×CAG)$^{X\text{-}ray}$]. The crystal structure shows multiple conformations for 1 × 1 nucleotide AA internal loops (anti−anti and syn−anti) that suggest fluxional behavior. To provide insight into these results and probe more deeply into the structure of the AA internal loops, MD simulations using the AMBER force field in explicit solvent were run on the model systems r(5′GCGCAGCGC)$_2$ (MS1), r(5′CCGCAGCGG)$_2$ (MS2), and r[5′GGGC(CAG)$_3$GUCC]$_2$ (3×CAG) including a detailed analysis of the dynamics of 1 × 1 nucleotide AA internal loops. After choosing two reaction coordinates, which mimic base flipping and base orientation with respect to sugar moieties for the 1 × 1 nucleotide AA internal loops, a 2D free energy landscape for syn−anti ↔ anti−anti transformation was generated by combining WHAM with umbrella sampling MD simulations. It was found that the AA base pairs are dynamic and can form stable structures both in anti−anti and syn−anti conformations with one hydrogen bond. The results indicate that the anti−anti and syn−anti 1 × 1 nucleotide AA internal loops are major and minor conformations, respectively. Multiple pathways are located for the syn−anti ↔ anti−anti transformation. Moreover, an electronegative binding pocket was determined around syn−anti AA base pairs where individual Na^+ ions can bind for as long as 50 ns. These results are important to better understand how r(CAG)^{exp} contributes to disease, as well as to assist in the design of small molecules that bind r(CAG)^{exp} and ameliorate disease.

METHODS

Crystallization and Structure Refinements. The RNA duplex, r[5UUGGGC(CAG)$_3$GUCC]$_2$ [r(3×CAG)$^{X\text{-}ray}$], at 1.2 mM concentration was dissolved in DEPC−water and folded by heating to 60 °C for 5 min and cooling to room temperature. A crystal of r(3×CAG)$^{X\text{-}ray}$ was grown by the sitting drop vapor diffusion method using 0.2 μL of 1.2 mM RNA and an equal volume of precipitants. The precipitants for r(3×CAG)$^{X\text{-}ray}$ were 15 mM $Mg(CH_3COO)_2$, 50 mM Na cacodylate, pH 6.0, 1.7 M $(NH_4)_2SO_4$. A diffraction data set with Bragg spacings to 1.65 Å for r(3×CAG)$^{X\text{-}ray}$ was collected on a MAR325 CCD detector at beamline 12−2 of the Stanford Synchrotron Radiation Laboratory. The data sets were integrated and scaled using HKL2000.[63] Phases for RNA structure were obtained by molecular replacement using Phaser[64] in the Phenix program interface[65] with PDB entry 3SYW as a search model. Crystallographic refinement was performed using Phenix,[65] and multiple rounds of manual model fittings were performed using Coot. Data collection and the crystallographic refinement statistics are summarized in Table 1. The crystal structure of r(3×CAG)$^{X\text{-}ray}$ has been deposited in Protein Data Bank under PDB code 4J50.

Preparation of Model Systems for MD Simulations. Model systems MS1, MS2, and 3×CAG (Figure 1) were prepared for MD simulations. MS1 and MS2 were modeled using the nucgen module of AMBER9[66] with AA base pairs in anti−anti and syn−anti conformations. 3×CAG (Figure 1) was modeled from crystal structure r(3×CAG)$^{X\text{-}ray}$ by trimming down the flanking uridines. In the model 3×CAG structure, one of the terminal AA base pairs was modified to be in anti−anti conformation. This was done because the crystal structure of r(3×CAG)$^{X\text{-}ray}$ is symmetric and has both the terminal AA base pairs in syn−anti conformations that puts redundancy to the analysis of potential syn−anti ↔ anti−anti transformations. The systems were neutralized with Na^+ ions[67] and solvated with TIP3P water molecules[68] in a truncated octahedral box. The MS1/MS2 and 3×CAG systems had 4025 and 8995 water molecules, respectively. The AMBER force field[28] with revised χ[69] and α/γ[70] torsional parameters was used in molecular dynamics and umbrella sampling simulations.

The main reason why the flanking uridine bases were removed from the structure was to mimic the in vivo r(CAG)^{exp}. In the crystallization process, flanking uridines were included in order to crystallize the Target RNA, which resulted in terminal AA base pairs in syn−anti conformations. The observation of this conformation, which was not seen before in RNA CAG repeats, motivated us to delve into the mechanism behind it. By trimming down the uridine bases, we disrupted the interaction between the flanking uridines and the terminal AA base pairs, giving us the opportunity to investigate the dynamics of AA base pairs when starting with syn−anti conformations in 3×CAG.

Molecular Dynamics Simulations. The systems were first minimized and equilibrated in two steps as described previously.[71,72] In the production runs, constant pressure dynamics with isotropic

dx.doi.org/10.1021/ja3108627 | J. Am. Chem. Soc. 2013, 135, 3528−3538

Table 1. Data Collection and Refinement Statistics

	r(3×CAG)$^{X\text{-ray}}$
Data Collection	
space group	*H*3
unit cell dimensions	
a, *b*, *c* (Å)	46.3, 46.3, 134.6
α, *β*, *γ* (deg)	90, 90, 120
resolution (Å)	50−1.65 (1.71−1.65)[a]
total measured refltns	228 869
unique refltns	12 952
R_{merge} (%)[b]	5.1 (49.5)[a]
$I/\sigma(I)$	40.4 (3.8)[a]
completeness (%)	99.8 (100.0)[a]
redundancy	5.7 (5.6)[a]
Refinement	
resolution (Å)	22.43−1.65 (1.82−1.65)[a]
no. of refltns	12 318
R_{work}[c]/R_{free}[d]	16.6/17.9 (18.9/17.9)[a]
no. of atoms	
RNA	808
ligand/ion	10
solvent	112
av *B*-factors	
RNA	50.5
ligand/ion	23.7
solvent	38.3
rmsd from ideal geometry	
bond lengths (Å)	0.004
bond angles (deg)	0.697

[a]Values in parentheses are for the highest resolution shell. [b]$R_{merge} = \sum_h\sum_i|I(h)_i - \langle I(h)\rangle|/\sum_h\sum_i I(h)_i$, where $I(h)_i$ is the *i*th observation of the reflection *h* and $\langle I(h)\rangle$ is the weighted average intensity for all observations *i* of reflection *h*. [c]$R_{work} = \sum_h||F_{obs}(h)| - |F_{cal}(h)||/\sum_h|F_{obs}(h)|$, where $F_{obs}(h)$ and $F_{cal}(h)$ are the observed and calculated structure factors for reflection *h*, respectively. [d]R_{free} was calculated as R_{work} using the 5% of reflections that were selected randomly and omitted from refinement.

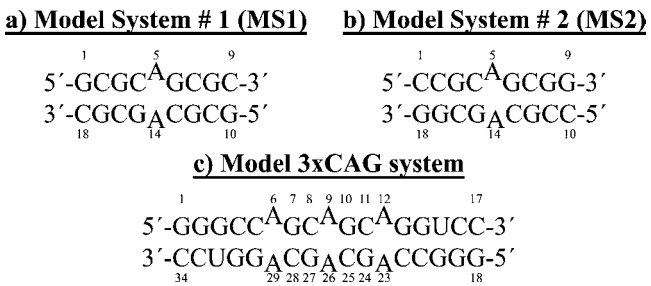

Figure 1. Sequences and structures of the RNA model systems used in molecular dynamics and umbrella sampling simulations.

positional scaling was used. The reference pressure was 1 atm with a pressure relaxation time of 2 ps. SHAKE[73] was turned on for bonds involving hydrogen atoms. An atom-based long-range hard cutoff of 8.0 Å was used in all simulations. A total of 854 and ∼500 ns of MD were run at 300 K with a 1 fs time step for 3×CAG and MS1/MS2, respectively. Simulations were carried out with the PMEMD module in AMBER9.[66] Trajectory files were written at each 5000 fs time step. For all these calculations, over 210K CPU hours were used.

Umbrella Sampling Simulations. In order to predict the potential pathways for the syn−anti ↔ anti−anti transformation, a 2D potential of mean force (PMF) surface was calculated for the model system MS2. Rotation around the glycosidic bond is responsible for the syn and anti base orientations of adenosine with respect to the adjacent sugar. As a result, the *χ* torsional angle was chosen as one of the reaction coordinates to mimic the base orientation (Figure 2a). A second reaction coordinate, called center-of-mass pseudodihedral angle (*θ*), was chosen to mimic unstacking of adenosine, as shown in Figure 2b. Similar reaction coordinates for base flipping studies of oligonucleotides were used previously.[60,61,74] Each reaction coordinate was rotated with an increment of 10°, yielding 36 × 36 = 1296 conformations. Initial structures with different (*χ*, *θ*) combinations were created for the model system MS2.

Minimization. Each structure was minimized in two steps: (1) All residues except the adenosines were held fixed with a restraint force of 10 kcal/mol Å^2. *χ* and *θ* dihedrals were held fixed in a particular combination using a square bottom well with parabolic sides that had force constants of 50 000 kcal/mol rad^2. A steepest descent minimization of 2000 steps was followed by a conjugate gradient minimization of 2000 steps. (2) Similar to the first step, the *χ* and *θ* dihedrals were held fixed in their initial combination. Watson−Crick base pairing restraints were imposed on the GC base pairs neighboring the 1 × 1 nucleotide AA internal loop. A steepest descent minimization of 25 000 steps was followed by a conjugate gradient minimization of 25 000 steps (Tables S1 and S2, Supporting Information).

Equilibration. After minimization, two steps of pressure equilibration were completed: (1) the RNA molecule was held fixed with a restraint force of 10 kcal/mol Å^2. Constant volume dynamics with an atom-based long-range hard cutoff of 8.0 Å was used. SHAKE[73] was turned on for bonds involving hydrogen atoms. The temperature was raised from 0 to 300 K in 20 ps. Langevin dynamics with a collision frequency of 1 ps^{-1} was used. A total of 20 ps of MD was run with a 2 fs time step. (2) The above conditions were chosen, except the following: *χ* and *θ* dihedrals were held fixed in their initial combination with a force constant of 500 kcal/mol rad^2. Watson−Crick base pairing restraints were imposed on GC base pairs neighboring 1 × 1 nucleotide AA internal loops. Constant pressure dynamics with isotropic positional scaling was turned on. The reference pressure was 1 atm with a pressure relaxation time of 2 ps. A total of 100 ps of MD was run with a 2 fs time step. Particle mesh Ewald (PME)[75,76] was used in all calculations.

Production Runs. Each production run was similar to the second step of the pressure equilibration described above. No restraints except the ones imposed on *χ* and *θ* dihedrals were used in the simulations. A square bottom well with parabolic sides was used to restrain *χ* and *θ* dihedrals with force constants of 50 kcal/mol rad^2. For each simulation, a total of 2 ns of MD was run with a 2 fs time step. (*χ*, *θ*) data were written at intervals of 10 fs. Simulations were carried out with the sander.MPI module in AMBER11. For umbrella sampling calculations, over 267K CPU hours were used.

Analysis. Dihedral and root-mean-square deviation (rmsd) analyses were completed using the ptraj module in the AMBER package.[66] The weighted histogram analysis method[77,78] (WHAM) was used to calculate the PMF surface using WHAM version 2.0.4 written by Grossfield (http://membrane.urmc.rochester.edu/content/wham). In the WHAM analysis, the last 1.5 ns data of each umbrella sampling simulation were used, and periodicity was turned on in both dimensions.

RESULTS AND DISCUSSION

Structure of r(3×CAG)$^{X\text{-ray}}$ [a model of r(CAG)^{exp}]. Figure 3A shows the secondary structure of an RNA construct that has three copies of the 5′CAG/GAC motif. The crystal structure was refined to 1.65 Å resolution [r(3×CAG)$^{X\text{-ray}}$]. The central 5′CAG/GAC region of r(3×CAG)$^{X\text{-ray}}$ is in the anti−anti 1 × 1 nucleotide AA internal loop conformation, while the terminal AA base pairs are in the syn−anti conformations (Figures 3B and 4). The duplex crystallized in double-stranded helical structure and made pseudoinfinite helices with the neighboring RNAs in the crystal lattice (Figure 3C). The duplex has A-form conformation and the overlay of

dx.doi.org/10.1021/ja3108627 | J. Am. Chem. Soc. 2013, 135, 3528−3538

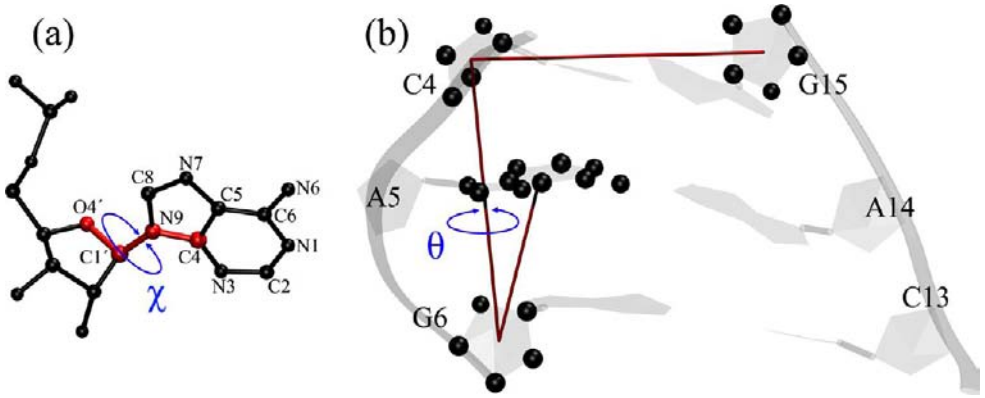

Figure 2. Reaction coordinates (χ and θ) used in PMF calculations for model system MS2 (Figure 1). χ torsional angle, O4′−C1′−N9−C4, is responsible for base orientation with respect to sugar (a). Center-of-mass (COM) pseudodihedral angle, θ, is chosen in order to mimic base unstacking of A with respect to the helical axis. θ is a pseudodihedral angle defined by COMs of four atom groups shown in part b.

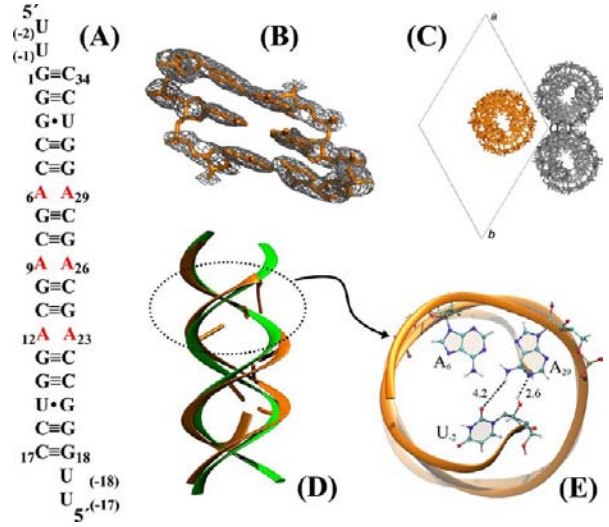

Figure 3. Secondary structure, refined structure, and crystal packing of the CAG repeat RNA construct [r(3×CAG)$^{X\text{-}ray}$]. (A) the secondary structure of the oligonucleotide 3×CAG duplex that was used for crystallization. (B) the central 5′-CA_8G/3′-$GA_{25}C$ of the RNA model structure for r(3×CAG)$^{X\text{-}ray}$. The electron density maps are contoured at 1.0 σ. (C) Illustration of crystal packing of r(3×CAG)$^{X\text{-}ray}$ (orange). Crystal packings shown in gray are crystallographic-symmetry-related molecules. Origin (O) and a- and b-axes are labeled accordingly. The c-axis is perpendicular to the plain of view. Each helix is extended to make a pseudoinfinite helix along the c-axis. (D) overlay of the backbone of r(3×CAG)$^{X\text{-}ray}$ (orange) onto the backbone of an ideal A-form RNA duplex (green) in which the 1 × 1 nucleotide AA internal loops and GU pairs are replaced with AU and GC pairs, respectively. Note that 5′-UU dangling ends interact with terminal AA base pairs from major groove sides in r(3×CAG)$^{X\text{-}ray}$. (E) Magnified image of A_6A_{29} pair to show interaction with U_{-2}. Note that the amino and 2′OH groups of A_{28} are in close contact with U_{-2}.

r(3×CAG)$^{X\text{-}ray}$ and A-form RNA shown in Figure 3D displays almost identical backbone structures except the 5′UU dangling ends, which interact with the terminal 1 × 1 nucleotide AA internal loops (Figure 3E). Amino and 2′-OH groups of A12 and A29 are in close contact with U_{-17} and U_{-2}, respectively, which cause A12 and A29 to adopt syn conformations (Figures 3E and 4). Almost all riboses are in C3′-*endo* conformation (sugar pucker) (Table S3, Supporting Information). Dihedral angle values for α, β, γ, δ, ε, and ζ can be found in Table S3 (Supporting Information). Parallel to Figure 3D, global helical parameters calculated for r(3×CAG)$^{X\text{-}ray}$ show characteristics of the A-form conformation with a minor groove width of 15.5 Å (Tables S4−S8, Supporting Information).

Electron density maps of individual 1 × 1 AA internal loops for r(3×CAG)$^{X\text{-}ray}$ are in line with syn−anti and anti−anti conformations for terminal and central 1 × 1 nucleotide AA internal loops, respectively (Figure 4). Temperature factor comparisons of the central anti−anti AA loop have higher average values in r(3×CAG)$^{X\text{-}ray}$ than base-paired regions (Figures 4 and S1, Supporting Information). This is evidenced by the well-defined electron density for base paired regions while the central 1 × 1 nucleotide AA internal loops have less well-defined electron density, indicating dynamic nature (Figures 4 and S1, Supporting Information). Electron densities for the CG closing base pairs are consistent with three hydrogen bonds (Figures S1 and S2, Supporting Information). Interestingly, a similar dynamic character has been observed in a refined X-ray structure of the 1 × 1 nucleotide UU internal loops in r(CUG)^{exp} models, suggesting that many repeats can sample multiple conformations.[19] In contrast, a refined X-ray structure of r(CGG) repeats shows that this RNA adopts a rather rigid structure, and each 1 × 1 nucleotide GG internal loop has a syn−anti conformation.[18]

Pathways for Syn−Anti ↔ Anti−Anti AA transformation. Umbrella sampling MD simulations were used to construct the 2D potential mean force (PMF) surface in order to visualize the potential pathways for the syn−anti ↔ anti−anti AA transformation (Figure 5). The x- and y-axes in Figure 5 are the reaction coordinates for unstacking (θ) and base orientation with respect to the sugar moiety (χ) of A5 in the 1 × 1 nucleotide AA internal loop (Figure 2). Three pathways are found for syn−anti ↔ anti−anti AA transformation (Figure 5). In path P1, A5 first unstacks from the helical axis through the minor groove direction (motion in x-axis). This motion relaxes the state and gives A5 enough space to make the syn ↔ anti transformation through a rotation around the glycosidic bond, χ (motion in y-axis). A5 then stacks back into the helical axis through the major groove direction to form the AA base pair. In P2, almost a direct syn ↔ anti transformation occurs in the system without A5 unstacking from the helical axis. In P3, a transformation similar to P1 is seen, except that unstacking occurs through the major groove direction. P1 has two energy barriers in the syn−anti transformation pathway with a stable local minimum at around (−75, 60) (Figure 5). In addition, P1 has a broader space in its transformation pathway compared to

dx.doi.org/10.1021/ja3108627 | J. Am. Chem. Soc. 2013, 135, 3528−3538

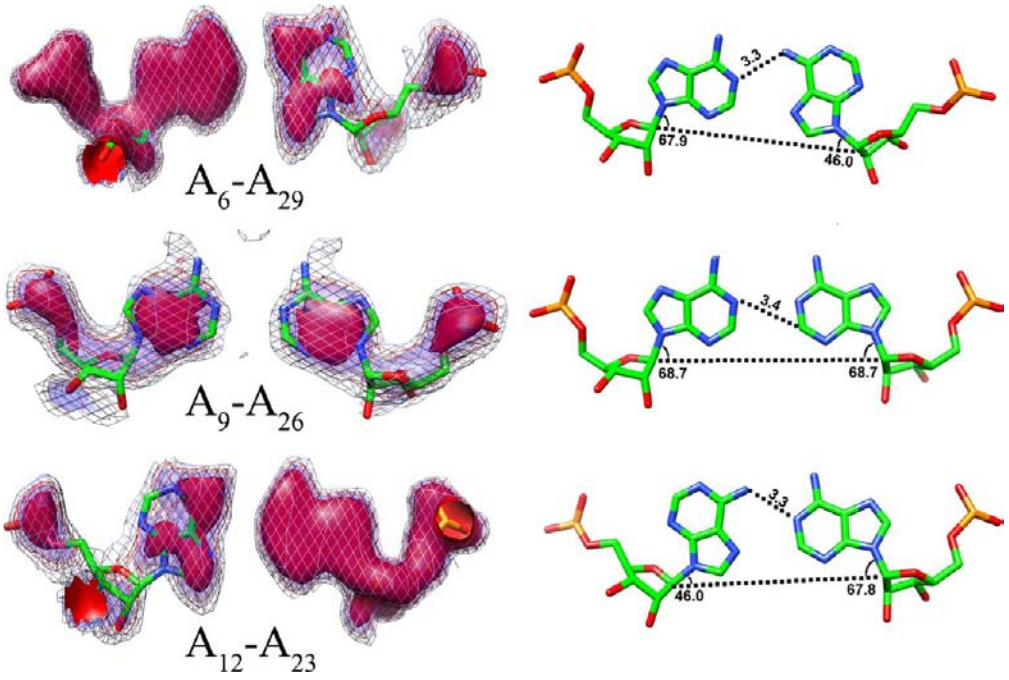

Figure 4. Stick models and electron densities of the 1 × 1 nucleotide AA internal loops for r(3×CAG)$^{X\text{-}ray}$. Electron density maps are contoured at 1.5 σ (red), 1.2 σ (blue), 1.0 σ (red mesh), and 0.6 σ (gray mesh). Hydrogen bonds, represented as dashed lines, and the distance values (in Å) are labeled.

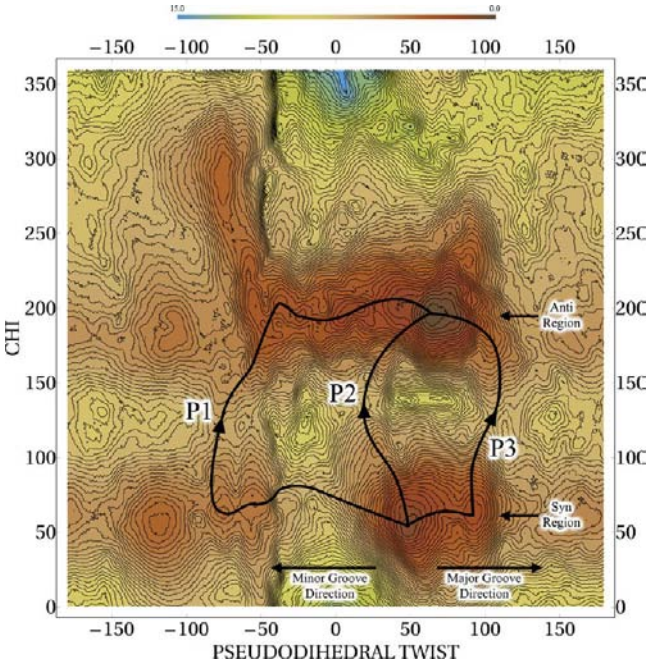

Figure 5. 2D PMF surface for model system MS2 showing the three pathways for syn−anti ↔ anti−anti AA transformation. The *x*- and *y*-axis are the reaction coordinates for stacking (θ) and base orientation with respect to sugar (χ) of adenosine, respectively (Figure 2). Anti and syn regions as well as the minor and major groove directions are shown. 1D free energy profiles of each pathway along the most likely direction are shown in Figures S3 and S4 (Supporting Information).

P2 and P3, which makes the transformation more probable. To explicitly show the differences between the pathways, 1D free energy profiles along the most likely direction for each path were extracted (Figures S3 and S4, Supporting Information). In Figure 5, the sampling range of the syn−anti region is very tight compared to the range of the anti−anti region. This means that the anti−anti region is dynamic and samples more than one conformation while syn−anti is much more rigid in structure compared to anti−anti.

In general, RNA loops are flexible, which gives them functional roles in the cell such as when AA base pairs form in RNA CAG repeats. This property, however, makes it hard to determine how small molecules bind to these flexible RNA regions, which was recently discussed by Al-Hashimi's group at the University of Michigan at Ann Arbor.[79] While Figure 5 discloses different potential pathways for the syn ↔ anti transformation, there are some results that should not be overlooked. RNA residues have three significant motions that affect the global RNA structure: (1) base opening/flipping, (2) base orientation with respect to sugar, and (3) sugar puckering. The first two motions will affect the RNA structure the most. In Figure 5, the *x*-axis represents base opening/flipping while the *y*-axis represents χ rotation. Even though the lowest energy regions are around (50, 50) (adenosine stacked on the helical axis in a syn conformation) and (60, 180) (adenosine stacked on the helical axis in an anti conformation) Figure 5 shows several other local minima regions in unstacked states such as around (−125, 50), (−125, 190), and (−75, 300). When AA base pairs are not interacting with anything, the structure prefers the anti−anti form, while upon interacting with something such as the flanking uridine bases they can adopt the syn−anti form. This interaction-driven conformational preference process can be applied to other local minima regions, too, as shown in Figure 5. It is possible that the local minima regions could be dominated by AA base pairs if a small molecule was designed to capitalize on these regions in binding to RNA.

Stability of Syn−Anti and Anti−Anti AA base pairs. Model systems MS1 and MS2 (Figure 1a,b) were designed in both syn−anti and anti−anti 1 × 1 nucleotide AA internal loop

dx.doi.org/10.1021/ja3108627 | J. Am. Chem. Soc. 2013, 135, 3528−3538

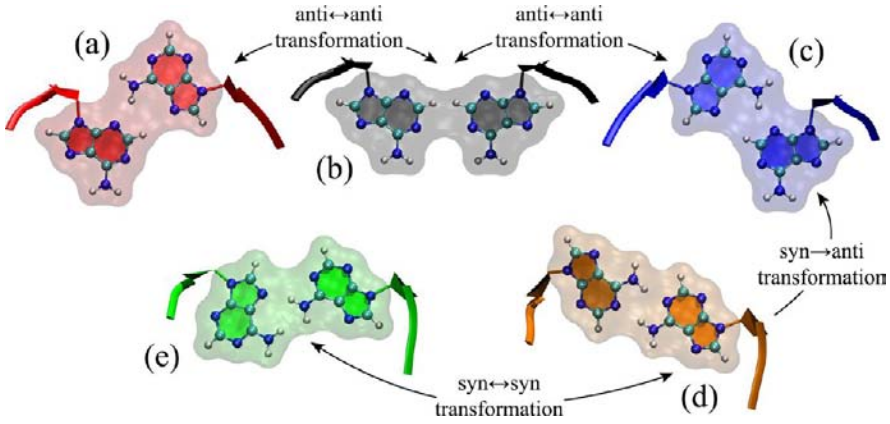

Figure 6. Different types of AA base pairings seen in MD simulations of model systems. Color notation was used to distinguish different AA types, which are also used in Figures 8, S5 and S6 (Supporting Information) to emphasize the type of transformations seen in the simulations. Arrow directions mean the type of transformations seen in the MD simulations. a–c have anti–anti AA conformation while d and e have syn–anti AA conformation. d is a transition state with two hydrogen-bonds seen in syn–anti → anti–anti AA transformation (3×CAG). No anti–anti → syn–anti AA transformation was seen, while multiple anti–anti ↔ anti–anti AA transformations were observed. Note that a and c are symmetric states.

conformations in order to investigate the dynamics. For each case, at least 500 ns MD simulations were run. Each system has a total of 16 Na^+ ions that neutralize the systems. Na^+ binding and rmsd analysis show unique properties for each conformation (see Figure S5, Supporting Information).

Rmsd of 1 × 1 nucleotide AA internal loops (with respect to initial conformations) and distances of each Na^+ ion from a loop as a function of time for each MD simulation were plotted (Figure S5, Supporting Information). In the MD simulations, different 1 × 1 nucleotide AA internal loop types were observed (Figures 6 and S5, Supporting Information). Different colors were used in Figure 6 to distinguish each 1 × 1 nucleotide AA internal loop type, and this color notation was conjoined with the rmsd analysis in Figure S5 (Supporting Information) to emphasize the structural transformations observed in the simulations. Additionally, different colors were used for each Na^+ ion in the Na^+ binding analysis to highlight the time spent by each ion around the 1 × 1 nucleotide AA internal loops (Figure S5, Supporting Information). It was observed that both syn–anti and anti–anti 1 × 1 nucleotide AA internal loop conformations were stable in these model systems. While the syn–anti 1 × 1 nucleotide AA internal loop remained in the initial configurations almost all the time, multiple anti–anti ↔ anti–anti 1 × 1 nucleotide AA internal loop transformations were observed (Figures 6 and S5, Supporting Information).

In the MD simulations that were started with syn–anti 1 × 1 nucleotide AA internal loop, there was a Na^+ binding pocket around the 1 × 1 nucleotide AA internal loop, which held different Na^+ ions throughout the simulations (Figures 7 and S5a1,b1, Supporting Information). Almost no structural change was seen in syn–anti AA base pair in these simulations. When 1 × 1 nucleotide AA internal loops were in syn–anti conformations, Na^+ ions were bound in this pocket for as long as over 50 ns (Figure S5, Supporting Information). In this state, Na^+ was interacting with the electronegative groups of anti-A and neighboring G (Figure 7). On average, distances between Na^+ and A-N7, G-N7, and G-O6 were 2.4, 2.6, and 3.3 Å, respectively (Figure 7). This Na^+-bound state is one reason why 1 × 1 nucleotide AA internal loop in the syn–anti conformation did not fluctuate too much from its initial state (Figure S5, Supporting Information). Indeed, when there were fluctuations in syn–anti 1 × 1 nucleotide AA loops in the MD

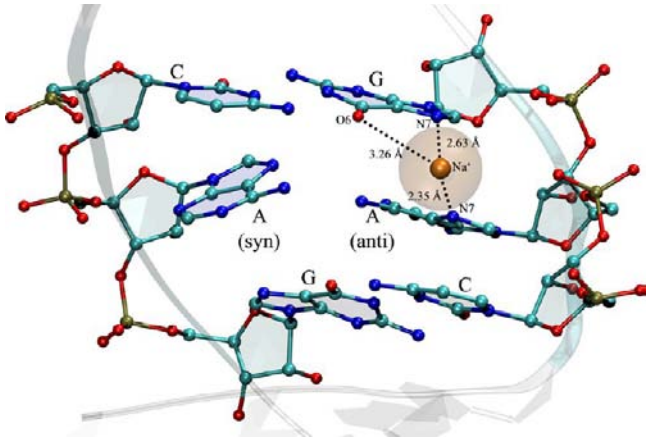

Figure 7. Na^+-bound state in syn–anti AA base pairs.

simulations, there were no Na^+ ions bound to this binding pocket (Figure S5a1,a2,b1,b2, Supporting Information). Around 125 and 440 ns in the MD simulation of model system MS1 (Figure S5a, Supporting Information) and around 325 ns in the MD simulation of model system MS2 (Figure S5b, Supporting Information), no Na^+ ions were bound in the pocket. At these times, syn–anti AA transformed to a transition state for a short period of time that corresponds to the orange-colored AA state shown in Figure 6d and highlighted with orange in the rmsd analysis (Figure S5a1,a2,b1,b2, Supporting Information). Thus, the dynamics of syn–anti 1 × 1 nucleotide AA internal loops were controlled by the Na^+ binding in this pocket.

In the MD simulations that were started with anti–anti 1 × 1 nucleotide AA internal loops, no Na^+ binding pocket was found (Figure S5c,d, Supporting Information). Na^+ ions were spending at most 10 ns around AA base pairs in these systems (Figure S5, Supporting Information). On average, a Na^+ ion was present within 5.5 Å of AA for 33% and 91% of the time in the anti–anti and syn–anti AA systems, respectively. The anti–anti 1 × 1 nucleotide AA internal loops, however, were dynamic. Multiple anti–anti ↔ anti–anti AA conformational transformations displayed in Figure 6 were observed in the simulations (Figure S5c,d, Supporting Information). This result is in line with the umbrella sampling predictions that span a

dx.doi.org/10.1021/ja3108627 | J. Am. Chem. Soc. 2013, 135, 3528–3538

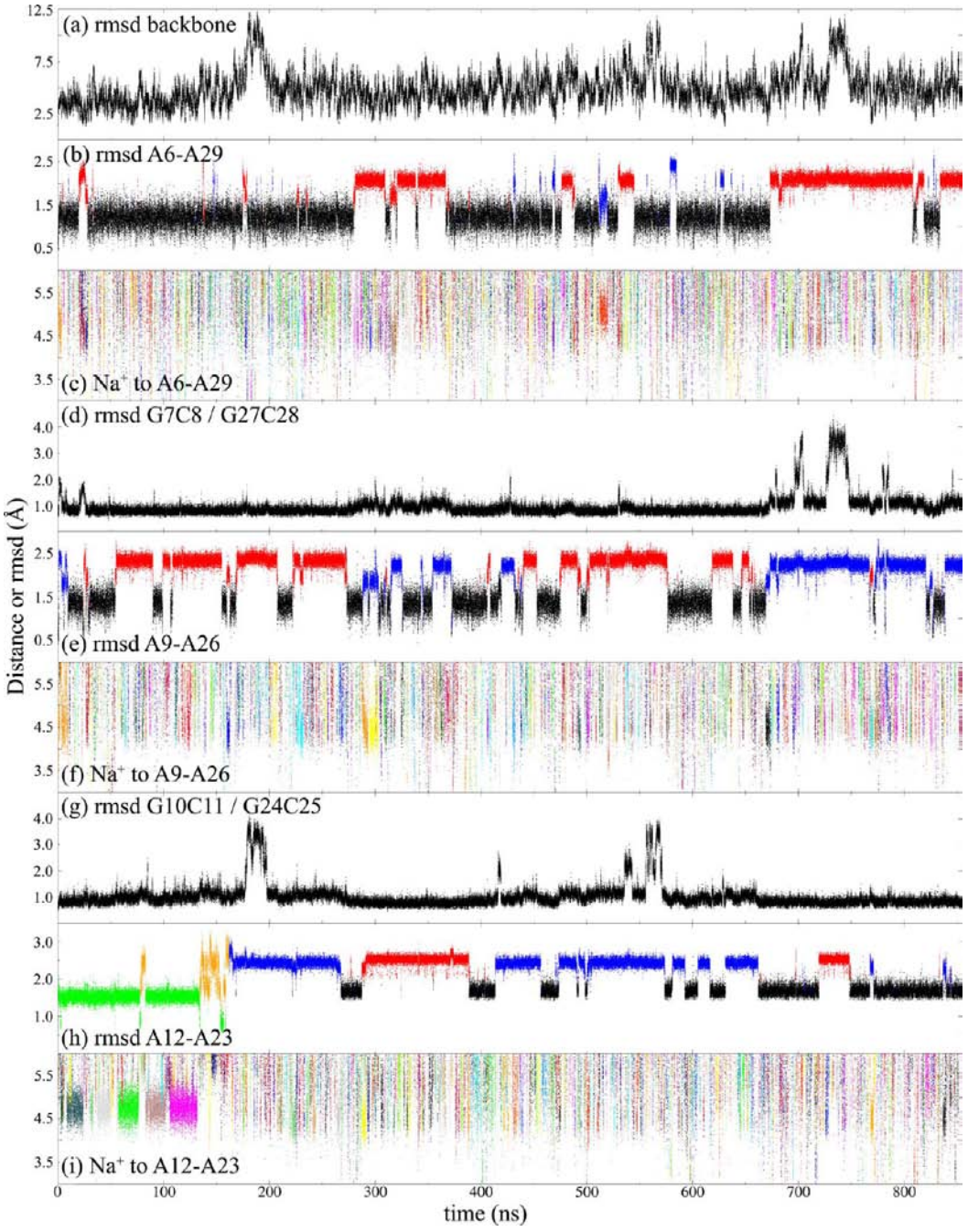

Figure 8. Rmsd and Na^+ binding analysis of 3×CAG MD simulation. Residue numbering defined in Figure 1c is used in the analysis. Rmsd (in Å) of (a) backbone, (b) A6-A29 base pair, (d) G7C8/G27C28, (e) A9-A26 base pair, (g) G10C11/G24C25, and (h) A12-A23 base pairs with respect to initial structure. The system has a total of 32 Na^+ ions highlighted with different colors, and distances (in Å) between each Na^+ ion to AA base pairs are plot in c, f, and i. In b, e, and h color schemes defined in Figure 6 for each AA type are used in order to highlight the transformations. Note that there is a Na^+ binding pocket when AA is in syn−anti conformation between 0 and 130 ns (i).

wide range for the anti−anti 1 × 1 nucleotide AA internal loops in the 2D PMF surface (Figure 5).

One explanation for not observing the syn−anti ↔ anti−anti AA transformation in these systems might be due to the energy barrier, which could be too high to overcome. In order to test this hypothesis, 10 independent temperature jump MD simulations were completed on model system MS2, which were started both in syn−anti and anti−anti 1 × 1 nucleotide AA internal loop conformations. The temperature in each MD simulation was gradually increased from 300 to 400 K within 20 ns without any restraints, and final structures were analyzed. Five out of ten MD simulations that started with syn−anti 1 × 1 nucleotide AA internal loops ended up in anti−anti 1 × 1 nucleotide AA internal loop conformation, while none of the simulations that started with anti−anti 1 × 1 nucleotide AA internal loops transformed to syn−anti AA. In model systems MS1 and MS2, there are four Watson−Crick GC base pairs on both sides of the 1 × 1 nucleotide AA internal loops, while in the original triplet $r(3\times CAG)^{X\text{-ray}}$ system there are only two GC base pairs between each consecutive 1 × 1 nucleotide AA internal loop. The results, therefore, suggest that model systems

dx.doi.org/10.1021/ja3108627 | J. Am. Chem. Soc. 2013, 135, 3528−3538

MS1 and MS2 have rigid stem regions that increase the energy barrier of the syn−anti ↔ anti−anti AA transformation.

Dynamics of Model 3×CAG system. Model 3×CAG system (Figure 1c) resembles the original triplet RNA, $r(3\times CAG)^{X\text{-}ray}$ (Figure 3a), much more than the model systems MS1 and MS2 (Figure 1a,b). As a result, the dynamics of 3×CAG was investigated by doing an 854 ns long MD simulation. There were a total of 32 Na^+ ions that neutralized the system.

A different rmsd and Na^+ binding analysis was completed on 3×CAG (Figure 8). As before, each individual Na^+ ion is highlighted with different colors (Figure 8c,f,i). Similar to the analysis completed for MS1 and MS2, the rmsd's of each 1 × 1 nucleotide AA internal loop with respect to initial conformation were plotted (Figure 8b,e,h). Colors representing unique 1 × 1 nucleotide AA internal loop types in Figure 6 were used in the rmsd analysis to emphasize the type of transformations seen in the MD simulation (Figure 8b,e,h). Moreover, the rms deviations of backbone and GC/CG stems located between the consecutive 1 × 1 nucleotide AA internal loops were plotted in order to investigate the rigidity of different regions of 3×CAG with respect to time (Figure 8a,d,g).

Similar to the results of MS1 and MS2, it was observed that there was a Na^+ binding pocket around the syn−anti type 1 × 1 nucleotide AA internal loop (see Figure 8i, first 125 ns). The initial conformation of A12-A23 was syn−anti, and this conformation was stable for the first 125 ns (Figure 8h). In this syn−anti state, different Na^+ ions were binding to the pocket for as long as 30 ns (Figure 8h,i). At around 175 ns, however, a full transformation from *syn*-A12−*anti*-A23 to *anti*-A12−*anti*-A23 was observed (Figure 8h). This structural transformation was initiated when there were no Na^+ ions bound to the pocket (Figure 8i). Without a Na^+ ion in the pocket, *syn*-A12 first unstacked through the minor groove side to transform itself into a transition state with two hydrogen bonds (Figure 6d and highlighted with orange color in Figure 8h). This particular transformation from the *syn*-A12−*anti*-A23 to the "transition state" *syn*-A12−*anti*-A23 was seen a couple of times in the first 175 ns (highlighted with orange in Figure 8h). At around 175 ns, *syn*-A12 transformed fully to *anti*-A12 to form the *anti*-A12−*anti*-A23 base pairing (Figure 8h). Once the A12-A23 base pair was in the anti−anti form, multiple anti−anti → anti−anti transformations were observed until the end of the MD simulation (Figures 6 and 8h).

In order to explicitly define the syn−anti → anti−anti transformation seen in the MD simulation, the (χ, θ) states occupied by A12 between 125 and 175 ns were plot (Figure S6, Supporting Information). The pathway P1 predicted by umbrella sampling calculations (Figure 5) was followed by A12 in the *syn*-A12−*anti*-A23 → *anti*-A12−*anti*-A23 transformation. Note that the prediction of pathway P1 for MS2 by umbrella sampling calculations is almost identical to the 3×CAG MD simulation result (Figures 5 and S6, Supporting Information).

The other two 1 × 1 nucleotide AA internal loops, A6-A29 and A9-A26, which were started in anti−anti conformations, never transformed to a syn−anti state. Similar to the results of MS1 and MS2, no Na^+ binding pocket was found when the 1 × 1 nucleotide AA internal loop was in the anti−anti conformation (Figure 8c,f). As before, multiple anti−anti ↔ anti−anti AA transformations were observed for these internal loops (Figure 8b,e).

Model 3×CAG is not as rigid as model systems MS1 and MS2. The two Watson−Crick GC/GC base pairs between each 1 × 1 nucleotide AA internal loop in 3×CAG were responsive to the environment. Rms deviations of G10C11/G24C25 at around 180 ns (right after the *syn*-A → *anti*-A transformation) and 560 ns and of G7C8/G27C28 at around 735 ns were over 3 Å (Figure 8d,g). These fluctuations have a direct effect on the RNA backbone, giving an rmsd over 10 Å during these times (Figure 8a). Such flexible neighbors around 1 × 1 nucleotide AA internal loops were not observed in the model systems MS1 and MS2 that may contribute to lowering the free energy barrier for the *syn*-A ↔ *anti*-A transformation.

Except for the transition state, all stable 1 × 1 nucleotide AA internal loops in the MD studies of 3×CAG, MS1, and MS2 have one hydrogen bond (Figure 6). These noncanonical pairs are weak compared to Watson−Crick base pairs, which have two or three hydrogen bonds.[80−82] As a result, any slight perturbation of the 1 × 1 nucleotide AA internal loop will have an effect on its conformation. Adenosine has three electronegative regions (N1, N3, N7) (Figure 2a) that can make noncovalent electrostatic interaction with cations such as Na^+ and molecules. In a 1 × 1 nucleotide AA internal loop with one hydrogen bond, there are a total of five free electronegative groups on the adenosine bases that can interact with Na^+ ions. Except for the Na^+ ions bound to the pocket in syn−anti AA, the ions spent only short amounts of time near these electronegative regions (Figures 8c,f,i and S5, Supporting Information). It was observed that, depending on the momentum of the ions, they could assist 1 × 1 nucleotide AA internal loops in the structural transformations represented in Figure 6 (Movies S1−S3, Supporting Information).

RNA CAG Loops in Literature. The 1 × 1 nucleotide AA internal loop conformations predicted by MD simulations (Figure 6) are also observed in RNA crystal structures. The Cate group at the University of California at Berkeley refined crystal structures of *Escherichia coli* ribosome bound to different complexes.[83−90] In these structures, there are 5′-C<u>A</u>G/3′-G<u>A</u>C motifs with syn−anti 1 × 1 nucleotide AA internal loop conformations. Yet, the ribosomal structure is much more complex compared to the 3×CAG duplex structure that is presented herein. Thus, different long-range interactions can play roles to alter the conformation of the 5′-C<u>A</u>G/3′-G<u>A</u>C motif in the ribosome. For example, in the bacterial ribosome the conformation of one of the terminal GC base pairs in a 5′-C<u>A</u>G/3′-G<u>A</u>C motif does not form a canonical GC paired structure due to the formation of a pseudoknot. In the crystal structure of the ribosome-bound cricket paralysis virus, the 5′-C<u>A</u>G/3′-G<u>A</u>C motif has anti−anti AA conformation that is similar to Figure 6a,c.[91] The crystal structure of $r(GGC\underline{A}GC\underline{A}GCC)_2$ has two 5′-C<u>A</u>G/3′-G<u>A</u>C motifs that have both 1 × 1 nucleotide AA internal loops in anti−anti form, similar to the structure presented in Figure 6b.[23] This crystal structure, however, has two sulfate (SO_4^{2-}) molecules that interact with the amino groups of 1 × 1 nucleotide AA internal loops to stabilize the conformation. This observation further suggests that the interaction of ions or small molecules can affect the structures of the 1 × 1 nucleotide internal loops in transcripts that contain expanded repeats in significant ways. These ligand-induced structural changes could also affect the binding of protein to these expanded repeats.

dx.doi.org/10.1021/ja3108627 | *J. Am. Chem. Soc.* 2013, 135, 3528−3538

SUMMARY AND CONCLUSIONS

Purines and pyrimidines have different electronic structures, and this difference brings different properties to their nucleotides. One such structural difference is seen in the preferred glycosidic dihedral angles, χ, which are responsible for the base orientation with respect to sugar. While pyrimidines prefer mostly the anti conformation, purines have a tendency to be in the syn state.[69] This main difference between pyrimidines and purines will have an affect on properties of different RNA triplet repeats. Recently, the χ torsional parameters for the AMBER force field were revised, yielding better structural and thermodynamic predictions for unique RNA systems.[69,71,72] Backed with the revised χ parameter sets, structural and thermodynamic calculations on other RNA triplet repeats such as CUG, CCUG, CCG, and CGG will produce important results that can be used against the genetic neurological diseases described above.

In this report, we described a refined crystal structure of r[5′UUGGGC(CAG)$_3$GUCC]$_2$ [r(3×CAG)$^{X\text{-}ray}$], a model of r(CAG)^{exp}, refined to 1.65 Å resolution. In conjunction with MD simulations, the structure showed that the 1 × 1 nucleotide AA internal loops sample anti−anti and syn−anti conformations. Moreover, the 1 × 1 nucleotide AA internal loops have structures that are sensitive to their environment. Our MD studies provide key insights to the properties of the AA internal loops. While the 1 × 1 nucleotide AA internal loops in r(3×CAG)$^{X\text{-}ray}$ repeats prefer the anti−anti conformation, the syn−anti form is another stable conformation. The latter conformation has structure that is affected and stabilized by a Na^+ binding pocket formed near this internal loop. Parallel to this result, the crystal structure shows dangling uridine bases stabilizing the syn−anti conformations. These studies thus suggest that a small molecule that binds to 1 × 1 nucleotide AA internal loops can affect conformation. Such information is useful in understanding the potential structural consequences of ligand binding to repeating transcripts and designing compounds that affect biological function.

For diseases caused by r(CAG)^{exp}, small molecules that can inhibit protein binding, thus modulating RNA gain-of-function toxicity and inhibit translation of toxic polyQ proteins, would be ideal. Both of these active areas of research[24,92−94] can be aided by a more thorough understanding of the structural nature of expanded repeats, including information about dynamics.

ASSOCIATED CONTENT

Supporting Information

Descriptions for each movie; minimization protocol and sample torsional restraint file used in umbrella sampling simulations; sugar and backbone torsional angles, distance and angle calculations for different base pairs, helical parameters calculated for base pairs and base pair steps, minor and major groove width calculations for r(3×CAG)$^{X\text{-}ray}$; electron densities and stick models of 1 × 1 AA loop closing CG base pairs; 1D free energy profiles along each pathway predicted by umbrella sampling calculations; Na^+ binding and rmsd analysis of AA base pairs for model systems MS1 and MS2; (χ, θ) states occupied by A12 in A12-A23 base pair in 3×CAG MD; stacking of AA internal loops on the loop closing CG base pairs in r(3×CAG)$^{X\text{-}ray}$; secondary structure, refined structure, and crystal packing of the CAG repeat RNA construct r-(3×CAG)$^{X\text{-}ray}$. This material is available free of charge via the Internet at http://pubs.acs.org.

AUTHOR INFORMATION

Corresponding Author

i-yildirim@northwestern.edu; schatz@chem.northwestern.edu; disney@scripps.edu

Notes

The authors declare no competing financial interest.

ACKNOWLEDGMENTS

We thank Dr. Amit Kumar for purification of materials, discussions, and review of the manuscript and Dr. Pengfei Fang and Dr. Min Guo of Scripps Research Institute for preliminary data. We thank Dr. Brent M. Znosko of Saint Louis University for helpful discussions. All computations were done at Advanced Research Computing (QUEST) at the Northwestern University and High Performance Computing (SEPA) at the Scripps Research Institute. Dr. Ilyas Yildirim thanks the Faculty of Science, Akdeniz University, Antalya, Turkey, for providing a working environment while he was in Turkey. This work was supported by NIH Grant 1R01GM079235-01A2 (MDD) and the PS-OC Center of the NIH/NCI Grant 1U54CA143869-01 (GCS).

[1]ABBREVIATIONS:

C, cytidine; G, guanosine; A, adenosine; QM, quantum mechanical; MM, molecular mechanics; MD, molecular dynamics; WHAM, weighted histogram analysis method; PMF, potential of mean force; PME, particle mesh Ewald; rmsd, root-mean-square deviation; MS1, r(5′GCGCAGCGC)$_2$; MS2, r(5′CCGCAGCGG)$_2$; 3×CAG, r[5′GGGC-(CAG)$_3$GUCC]$_2$; r(3×CAG)$^{X\text{-}ray}$, r[5′UUGGGC-(CAG)$_3$GUCC]$_2$

REFERENCES

(1) Ashley, C. T.; Warren, S. T. *Annu. Rev. Genet.* **1995**, *29*, 703.
(2) Emery, A. E. H. *Lancet* **2002**, *359*, 687.
(3) Sellier, C.; Rau, F.; Liu, Y. L.; Tassone, F.; Hukema, R. K.; Gattoni, R.; Schneider, A.; Richard, S.; Willemsen, R.; Elliott, D. J.; Hagerman, P. J.; Charlet-Berguerand, N. *EMBO J.* **2010**, *29*, 1248.
(4) Greco, C. M.; Berman, R. F.; Martin, R. M.; Tassone, F.; Schwartz, P. H.; Chang, A.; Trapp, B. D.; Iwahashi, C.; Brunberg, J.; Grigsby, J.; Hessl, D.; Becker, E. J.; Papazian, J.; Leehey, M. A.; Hagerman, R. J.; Hagerman, P. J. *Brain* **2006**, *129*, 243.
(5) Jin, P.; Duan, R. H.; Qurashi, A.; Qin, Y. L.; Tian, D. H.; Rosser, T. C.; Liu, H. J.; Feng, Y.; Warren, S. T. *Neuron* **2007**, *55*, 556.
(6) Verheij, C.; Bakker, C. E.; Degraaff, E.; Keulemans, J.; Willemsen, R.; Verkerk, A.; Galjaard, H.; Reuser, A. J. J.; Hoogeveen, A. T.; Oostra, B. A. *Nature* **1993**, *363*, 722.
(7) Verkerk, A.; Pieretti, M.; Sutcliffe, J. S.; Fu, Y. H.; Kuhl, D. P. A.; Pizzuti, A.; Reiner, O.; Richards, S.; Victoria, M. F.; Zhang, F. P.; Eussen, B. E.; Vanommen, G. J. B.; Blonden, L. A. J.; Riggins, G. J.; Chastain, J. L.; Kunst, C. B.; Galjaard, H.; Caskey, C. T.; Nelson, D. L.; Oostra, B. A.; Warren, S. T. *Cell* **1991**, *65*, 905.
(8) Klockgether, T.; Paulson, H. *Mov. Disord.* **2011**, *26*, 1134.
(9) Orr, H. T.; Zoghbi, H. Y. *Annu. Rev. Neurosci.* **2007**, *30*, 575.
(10) Shoulson, I.; Young, A. B. *Mov. Disord.* **2011**, *26*, 1127.
(11) Walker, F. O. *Lancet* **2007**, *369*, 218.
(12) Yazawa, I.; Nukina, N.; Hashida, H.; Goto, J.; Yamada, M.; Kanazawa, I. *Nat. Genet.* **1995**, *10*, 99.
(13) Li, L. B.; Yu, Z. M.; Teng, X. Y.; Bonini, N. M. *Nature* **2008**, *453*, 1107.
(14) Li, L. B.; Bonini, N. M. *Trends Neurosci.* **2010**, *33*, 292.

(15) Mykowska, A.; Sobczak, K.; Wojciechowska, M.; Kozlowski, P.; Krzyzosiak, W. J. *Nucleic Acids Res.* **2011**, *39*, 8938.
(16) Zu, T.; Gibbens, B.; Doty, N. S.; Gomes-Pereira, M.; Huguet, A.; Stone, M. D.; Margolis, J.; Peterson, M.; Markowski, T. W.; Ingram, M. A. C.; Nan, Z.; Forster, C.; Low, W. C.; Schoser, B.; Somia, N. V.; Clark, H. B.; Schmechel, S.; Bitterman, P. B.; Gourdon, G.; Swanson, M. S.; Moseley, M.; Ranum, L. P. W. *Proc. Natl. Acad. Sci. U. S. A.* **2011**, *108*, 260.
(17) Sobczak, K.; Michlewski, G.; de Mezer, M.; Kierzek, E.; Krol, J.; Olejniczak, M.; Kierzek, R.; Krzyzosiak, W. J. *J. Biol. Chem.* **2010**, *285*, 12755.
(18) Kumar, A.; Fang, P. F.; Park, H.; Guo, M.; Nettles, K. W.; Disney, M. D. *ChemBioChem* **2011**, *12*, 2140.
(19) Kumar, A.; Park, H.; Fang, P. F.; Parkesh, R.; Guo, M.; Nettles, K. W.; Disney, M. D. *Biochemistry* **2011**, *50*, 9928.
(20) Mooers, B. H. M.; Logue, J. S.; Berglund, J. A. *Proc. Natl. Acad. Sci. U. S. A.* **2005**, *102*, 16626.
(21) Parkesh, R.; Fountain, M.; Disney, M. D. *Biochemistry* **2011**, *50*, 599.
(22) Kiliszek, A.; Kierzek, R.; Krzyzosiak, W. J.; Rypniewski, W. *Nucleic Acids Res.* **2009**, *37*, 4149.
(23) Kiliszek, A.; Kierzek, R.; Krzyzosiak, W. J.; Rypniewski, W. *Nucleic Acids Res.* **2010**, *38*, 8370.
(24) Kumar, A.; Parkesh, R.; Sznajder, L. J.; Childs-Disney, J. L.; Sobczak, K.; Disney, M. D. *ACS Chem. Biol.* **2012**, *7*, 496.
(25) Parkesh, R.; Childs-Disney, J. L.; Nakamori, M.; Kumar, A.; Wang, E.; Wang, T.; Hoskins, J.; Tran, T.; Housman, D.; Thornton, C. A.; Disney, M. D. *J. Am. Chem. Soc.* **2012**, *134*, 4731.
(26) Krzyzosiak, W. J.; Sobczak, K.; Wojciechowska, M.; Fiszer, A.; Mykowska, A.; Kozlowski, P. *Nucleic Acids Res.* **2012**, *40*, 11.
(27) Malhotra, A.; Harvey, S. C. *J. Mol. Biol.* **1994**, *240*, 308.
(28) Cornell, W. D.; Cieplak, P.; Bayly, C. I.; Gould, I. R.; Merz, K. M.; Ferguson, D. M.; Spellmeyer, D. C.; Fox, T.; Caldwell, J. W.; Kollman, P. A. *J. Am. Chem. Soc.* **1995**, *117*, 5179.
(29) Brooks, B. R.; Bruccoleri, R. E.; Olafson, B. D.; States, D. J.; Swaminathan, S.; Karplus, M. *J. Comput. Chem.* **1983**, *4*, 187.
(30) MacKerell, J., A. D., Brooks, B., Brooks, III, C. L., Nilsson, L., Roux, B., Won, Y., and Karplus, M. In *The Encyclopedia of Computational Chemistry*; Schleyer, P. v. R., Allinger, N. L., Clark, T., Gasteiger, J., Kollman, P. A., Schaefer, I., H. F., Schreiner, P. R., Eds.; John Wiley & Sons: Chichester, 1998; Vol. *1*, p 271.
(31) Scott, W. R. P.; Hunenberger, P. H.; Tironi, I. G.; Mark, A. E.; Billeter, S. R.; Fennen, J.; Torda, A. E.; Huber, T.; Kruger, P.; van Gunsteren, W. F. *J. Phys. Chem. A* **1999**, *103*, 3596.
(32) Hobza, P.; Sponer, J. *J. Am. Chem. Soc.* **2002**, *124*, 11802.
(33) Kratochvil, M.; Sponer, J.; Hobza, P. *J. Am. Chem. Soc.* **2000**, *122*, 3495.
(34) Nam, K. H.; Gao, J. L.; York, D. M. *J. Am. Chem. Soc.* **2008**, *130*, 4680.
(35) Bash, P. A.; Field, M. J.; Karplus, M. *J. Am. Chem. Soc.* **1987**, *109*, 8092.
(36) Eichinger, M.; Tavan, P.; Hutter, J.; Parrinello, M. *J. Chem. Phys.* **1999**, *110*, 10452.
(37) Freindorf, M.; Gao, J. L. *J. Comput. Chem.* **1996**, *17*, 386.
(38) Gao, J. L.; Xia, X. F. *Science* **1992**, *258*, 631.
(39) Murphy, R. B.; Philipp, D. M.; Friesner, R. A. *J. Comput. Chem.* **2000**, *21*, 1442.
(40) Stanton, R. V.; Hartsough, D. S.; Merz, K. M. *J. Phys. Chem.* **1993**, *97*, 11868.
(41) Tunon, I.; MartinsCosta, M. T. C.; Millot, C.; RuizLopez, M. F.; Rivail, J. L. *J. Comput. Chem.* **1996**, *17*, 19.
(42) Duan, Y.; Kollman, P. A. *Science* **1998**, *282*, 740.
(43) Klepeis, J. L.; Lindorff-Larsen, K.; Dror, R. O.; Shaw, D. E. *Curr. Opin. Struct. Biol.* **2009**, *19*, 120.
(44) Maragakis, P.; Lindorff-Larsen, K.; Eastwood, M. P.; Dror, R. O.; Klepeis, J. L.; Arkin, I. T.; Jensen, M. O.; Xu, H. F.; Trbovic, N.; Friesner, R. A.; Palmer, A. G.; Shaw, D. E. *J. Phys. Chem. B* **2008**, *112*, 6155.
(45) Shaw, D. E.; Deneroff, M. M.; Dror, R. O.; Kuskin, J. S.; Larson, R. H.; Salmon, J. K.; Young, C.; Batson, B.; Bowers, K. J.; Chao, J. C.; Eastwood, M. P.; Gagliardo, J.; Grossman, J. P.; Ho, C. R.; Ierardi, D. J.; Kolossvary, I.; Klepeis, J. L.; Layman, T.; McLeavey, C.; Moraes, M. A.; Mueller, R.; Priest, E. C.; Shan, Y. B.; Spengler, J.; Theobald, M.; Towles, B.; Wang, S. C. *Commun. ACM* **2008**, *51*, 91.
(46) Zagrovic, B.; Pande, V. *J. Comput. Chem.* **2003**, *24*, 1432.
(47) Beveridge, D. L.; McConnell, K. J. *Curr. Opin. Struct. Biol.* **2000**, *10*, 182.
(48) Cheatham, T. E. *Curr. Opin. Struct. Biol.* **2004**, *14*, 360.
(49) Giudice, E.; Lavery, R. *Acc. Chem. Res.* **2002**, *35*, 350.
(50) Orozco, M.; Perez, A.; Noy, A.; Luque, F. J. *Chem. Soc. Rev.* **2003**, *32*, 350.
(51) Perez, A.; Blas, J. R.; Rueda, M.; Lopez-Bes, J. M.; de la Cruz, X.; Orozco, M. *J. Chem. Theory Comput.* **2005**, *1*, 790.
(52) Vokacova, Z.; Budesinsky, M.; Rosenberg, I.; Schneider, B.; Sponer, J.; Sychrovsky, V. *J. Phys. Chem. B* **2009**, *113*, 1182.
(53) Kumar, S.; Bouzida, D.; Swendsen, R. H.; Kollman, P. A.; Rosenberg, J. M. *J. Comput. Chem.* **1992**, *13*, 1011.
(54) Souaille, M.; Roux, B. *Comput. Phys. Commun.* **2001**, *135*, 40.
(55) Bartels, C.; Karplus, M. *J. Comput. Chem.* **1997**, *18*, 1450.
(56) Virnau, P.; Muller, M. *J. Chem. Phys.* **2004**, *120*, 10925.
(57) Babin, V.; Roland, C.; Darden, T. A.; Sagui, C. *J. Chem. Phys.* **2006**, *125*, 204909.
(58) Kastner, J. *Wiley Interdiscip. Rev.-Comput. Mol. Sci.* **2011**, *1*, 932.
(59) Giudice, E.; Varnai, P.; Lavery, R. *Nucleic Acids Res.* **2003**, *31*, 1434.
(60) Banavali, N. K.; MacKerell, A. D. *J. Mol. Biol.* **2002**, *319*, 141.
(61) Song, K.; Campbell, A. J.; Bergonzo, C.; de los Santos, C.; Grollman, A. P.; Simmerling, C. *J. Chem. Theory Comput.* **2009**, *5*, 3105.
(62) Hart, K.; Nystrom, B.; Ohman, M.; Nilsson, L. *RNA* **2005**, *11*, 609.
(63) Otwinowski, Z.; Minor, W. *Macromol. Crystallogr., Part A* **1997**, *276*, 307.
(64) Storoni, L. C.; McCoy, A. J.; Read, R. J. *Acta Crystallogr. D Biol. Crystallogr.* **2004**, *60*, 432.
(65) Adams, P. D.; Grosse-Kunstleve, R. W.; Hung, L. W.; Ioerger, T. R.; McCoy, A. J.; Moriarty, N. W.; Read, R. J.; Sacchettini, J. C.; Sauter, N. K.; Terwilliger, T. C. *Acta Crystallogr. D Biol. Crystallogr.* **2002**, *58*, 1948.
(66) Case, D. A.; Darden, T. A.; Cheatham, T. E. I.; Simmerling, C. L.; Wang, J.; Duke, R. E.; Luo, R.; Merz, K. M.; Pearlman, D. A.; Crowley, M.; Walker, R. C.; Zhang, W.; Wang, B.; Hayik, S.; Roitberg, A.; Seabra, G.; Wong, K. F.; Paesani, F.; Wu, X.; Brozell, S.; Tsui, V.; Gohlke, H.; Yang, L.; Tan, C.; Mongan, J.; Hornak, V.; Cui, G.; Beroza, P.; Mathews, D. H.; Schafmeister, C.; Ross, W. S.; Kollman, P. A. University of California—San Francisco: San Francisco, CA, 2006.
(67) Joung, I. S.; Cheatham, T. E. *J. Phys. Chem. B* **2008**, *112*, 9020.
(68) Jorgensen, W. L.; Chandrasekhar, J.; Madura, J. D.; Impey, R. W.; Klein, M. L. *J. Chem. Phys.* **1983**, *79*, 926.
(69) Yildirim, I.; Stern, H. A.; Kennedy, S. D.; Tubbs, J. D.; Turner, D. H. *J. Chem. Theory Comput.* **2010**, *6*, 1520.
(70) Perez, A.; Marchan, I.; Svozil, D.; Sponer, J.; Cheatham, T. E.; Laughton, C. A.; Orozco, M. *Biophys. J.* **2007**, *92*, 3817.
(71) Yildirim, I.; Stern, H. A.; Tubbs, J. D.; Kennedy, S. D.; Turner, D. H. *J. Phys. Chem. B* **2011**, *115*, 9261.
(72) Yildirim, I.; Kennedy, S. D.; Stern, H. A.; Hart, J. M.; Kierzek, R.; Turner, D. H. *J. Chem. Theory Comput.* **2012**, *8*, 172.
(73) Ryckaert, J. P.; Ciccotti, G.; Berendsen, H. J. C. *J. Comput. Phys.* **1977**, *23*, 327.
(74) Priyakumar, U. D.; MacKerell, A. D. *Chem. Rev.* **2006**, *106*, 489.
(75) Sagui, C.; Pedersen, L. G.; Darden, T. A. *J. Chem. Phys.* **2004**, *120*, 73.
(76) Toukmaji, A.; Sagui, C.; Board, J.; Darden, T. *J. Chem. Phys.* **2000**, *113*, 10913.
(77) Roux, B. *Comput. Phys. Commun.* **1995**, *91*, 275.
(78) Kumar, S.; Rosenberg, J. M.; Bouzida, D.; Swendsen, R. H.; Kollman, P. A. *J. Comput. Chem.* **1995**, *16*, 1339.

(79) Stelzer, A. C.; Frank, A. T.; Kratz, J. D.; Swanson, M. D.; Gonzalez-Hernandez, M. J.; Lee, J.; Andricioaei, I.; Markovitz, D. M.; Al-Hashimi, H. M. *Nat. Chem. Biol.* **2011**, *7*, 553.
(80) Davis, A. R.; Znosko, B. M. *Biochemistry* **2007**, *46*, 13425.
(81) Davis, A. R.; Znosko, B. M. *Biochemistry* **2010**, *49*, 8669.
(82) Davis, A. R.; Kirkpatrick, C. C.; Znosko, B. M. *Nucleic Acids Res.* **2011**, *39*, 1081.
(83) Berk, V.; Zhang, W.; Pai, R. D.; Cate, J. H. D. *Proc. Natl. Acad. Sci. U. S. A.* **2006**, *103*, 15830.
(84) Borovinskaya, M. A.; Pai, R. D.; Zhang, W.; Schuwirth, B. S.; Holton, J. M.; Hirokawa, G.; Kaji, H.; Kaji, A.; Cate, J. H. D. *Nat. Struct. Mol. Biol.* **2007**, *14*, 727.
(85) Borovinskaya, M. A.; Shoji, S.; Fredrick, K.; Cate, J. H. D. *RNA* **2008**, *14*, 1590.
(86) Borovinskaya, M. A.; Shoji, S.; Holton, J. M.; Fredric, K.; Cate, J. H. D. *ACS Chem. Biol.* **2007**, *2*, 545.
(87) Dunkle, J. A.; Xiong, L.; Mankin, A. S.; Cate, J. H. D. *Proc. Natl. Acad. Sci. U. S. A.* **2010**, *107*, 17152.
(88) Llano-Sotelo, B.; Dunkle, J.; Klepacki, D.; Zhang, W.; Fernandes, P.; Cate, J. H. D.; Mankin, A. S. *Antimicrob. Agents Chemother.* **2010**, *54*, 4961.
(89) Schuwirth, B. S.; Borovinskaya, M. A.; Hau, C. W.; Zhang, W.; Vila-Sanjurjo, A.; Holton, J. M.; Cate, J. H. D. *Science* **2005**, *310*, 827.
(90) Schuwirth, B. S.; Day, J. M.; Hau, C. W.; Janssen, G. R.; Dahlberg, A. E.; Cate, J. H. D.; Vila-Sanjurjo, A. *Nat. Struct. Mol. Biol.* **2006**, *13*, 879.
(91) Schueler, M.; Connell, S. R.; Lescoute, A.; Giesebrecht, J.; Dabrowski, M.; Schroeer, B.; Mielke, T.; Penczek, P. A.; Westhof, E.; Spahn, C. M. T. *Nat. Struct. Mol. Biol.* **2006**, *13*, 1092.
(92) Pushechnikov, A.; Lee, M. M.; Childs-Disney, J. L.; Sobczak, K.; French, J. M.; Thornton, C. A.; Disney, M. D. *J. Am. Chem. Soc.* **2009**, *131*, 9767.
(93) Hu, J. X.; Matsui, M.; Corey, D. R. In *Oligonucleotide Therapeutics*; Rossi, J. J., Gait, M. J., Eckstein, F., Eds.; 2009; Vol. *1175*, p 24.
(94) Hu, J. X.; Matsui, M.; Gagnon, K. T.; Schwartz, J. C.; Gabillet, S.; Arar, K.; Wu, J.; Bezprozvanny, I.; Corey, D. R. *Nat. Biotechnol.* **2009**, *27*, 478.